

Assessment of Some Experimental and Processing Factors for Background Oriented Schlieren Measurements

Ardian B. Gojani
Shigeru Obayashi

Institute of Fluid Science
Tohoku University
2-1-1 Katahira, Aoba, Sendai 980-8577
Japan
gojani@edge.ifs.tohoku.ac.jp

Abstract

An outline of background oriented schlieren (BOS) and its application to two types of flow is given. Extraction of quantitative data from the images depend on a number of factors, which are influenced from instrumentation and experimental adjustments, as well as from the image analysis and post-processing. These effects are investigated,

Key words: flow visualization, background oriented schlieren, sensitivity, error analysis.

Introduction

The problem we would like to address is the extraction of quantitative data from flow visualization, in particular from background oriented schlieren (BOS) technique. The technique was proposed and its fundamentals outlined in references [1] and [2], and a broad assessment is given in [3]. In BOS, a flow is made visible by comparing images of the flow in two different states, with each state being defined by a different distribution of flow properties. Since there exists a direct relationship between fluid flow properties and the fluid's refractive index, for gases explicitly expressed by the Gladstone-Dale equation, as a result, light rays will bend (refract) into two different directions, yielding a distorted image of the field of view.

Since its beginnings, flow visualization has mainly been concerned with qualitative description of the flow [4], while quantitative measurements were carried only in some limiting cases, mainly for two reasons:

1. quantitative measurements were impossible, e. g. shadowgraphy records the illumination change due to the second derivative of the density, which is impossible to be double integrated and give density values, or
2. quantitative measurements were too difficult and/or inaccurate compared to other techniques, e. g. interferometry.

The development of digital image processing and analysis has made possible new investigations into quantitative flow visualization. An outcome of these investigations is BOS, which makes use of a combination of standard photography and of cross-correlation methods of image analysis, as developed for laser speckle photography and particle image velocimetry.

In general, any type of background that shows locally illumination value differences may be used as a field of view for BOS visualization. For example, in references [5], the natural landscape full of features, mainly grass and trees, has been used as the field of view. A variant of BOS that makes use of backgrounds with specific features, prepared according to the requirements of the experiment, sometimes is referred as synthetic schlieren [6].

The present paper will argue that BOS can be used for quantitative measurements of the flow field, and, in line with [7] and [8], will investigate the accuracy of the technique as applied to synthetic images. Also, experimental results for two types of flows will be presented, showing the potential and limitations of the technique.

BOS technique

The principle of BOS lays in the difference between two images of the same pattern imaged through a test fluid: a reference image is taken without and a measurement image with a disturbance in the fluid that is to be evaluated, as illustrated in Fig. 1. The figure shows a side view of a BOS arrangement with the imaged background pattern B, the test section T (phase object with refractive index gradient $\partial n(\mathbf{r})/\partial y$), the objective lens L, and image plan, coplanar with the recording sensor, I. The angle of deflection due to the gradient of refractive index $n(\mathbf{r})$ is ε . Distances a , w , d between different sections of the BOS system, as well as the object and image distances s_o and s_i , respectively, are also noted. The recorded dot shift in the image plane is dy_i and its apparent shift in the background is dy_o . The full line along the optical axis is the light ray when a reference image is being taken, while the dashed line shows the ray during the measurement imaging in the presence of a fluid disturbance. The disturbance, e. g. a shock or a heat wave, causes local changes of density, resulting in changes of the refractive index. Hence, an imaging light beam passing through the disturbance will deflect and the angle of deflection is encoded in the difference between the measurement and the reference image. The equation that tracks the position of the ray is

$$\frac{d}{ds} \left(n(\mathbf{r}) \frac{d\mathbf{r}}{ds} \right) = \nabla n(\mathbf{r}) \quad , \quad (1)$$

where $\mathbf{r}(s)$ is the position vector representing the position of any point in the ray, $n=n(\mathbf{r})$ is the refractive index of the medium through which the ray passes, and ds is the infinitesimal arc length. From Eq. (1), considering plane $x=0$, and assuming paraxial approximation along optical axis z and negligible ray deviations – but, non-negligible change of ray's curvature, the angle of deflection along direction y is

$$\varepsilon_y = \int_a^{a+w} \frac{1}{n} \frac{\partial n}{\partial y} dz \quad , \quad (2)$$

with a and $a+w$ the entry and exit points in the phase object. This angle, and subsequently the refractive index, can be extracted, for example, by cross-correlation or ray tracing algorithms, enabling the deduction of the fluid's density from the relationship between the density and the refractive index. This relationship is given by the Gladstone-Dale relation

$$n - 1 = K \rho \quad , \quad (3)$$

where K is a constant of the medium and $\rho = \rho(\mathbf{r})$ is the density. Combination of Eqs. (1) and (3) gives the density field of the disturbance.

A BOS measurement consists of two stages: image recording and image evaluation. Image recording constitutes the choice of the background pattern, the recording system, i. e. cameras and lighting, and their arrangement. The background is characterized by two numbers: dot size and dot density, which are determined based on the pixel size and pixel count of the camera sensor. BOS' light capturing unit is an image sensor (CCD or CMOS based camera), characterized by its pixel count N_{px} and size Δ_{px} . Since the phenomena for which BOS is used are transient, the recording system needs to be fast enough to freeze the motion of the fluid under investigation. In general, sensors with large pixel count and pixel size take images with better quality, but the increase of these two parameters means that the field of view also needs to be large. Given a sensor with a certain pixel count and size, or alternatively a fixed field of view corresponding to the test section, the imaged dimensions of the fluid under study can be adjusted mainly through optical arrangement of the setup by setting distances a and d .

Image evaluation constitutes the comparison of reference and measurement image data and usually is done by using cross-correlation algorithms. The recorded images are a set of data that are divided into smaller sections, representing the interrogation windows. For an image recording done properly, the interrogation window of the reference and measurement images will have the same number of dots and with the same relative distances to each other, but shifted in reference to the absolute position. Correlation algorithms result in a peak that corresponds to the average dot shift in the image plane, with a resolution down to 0.1 pixels, achieved by

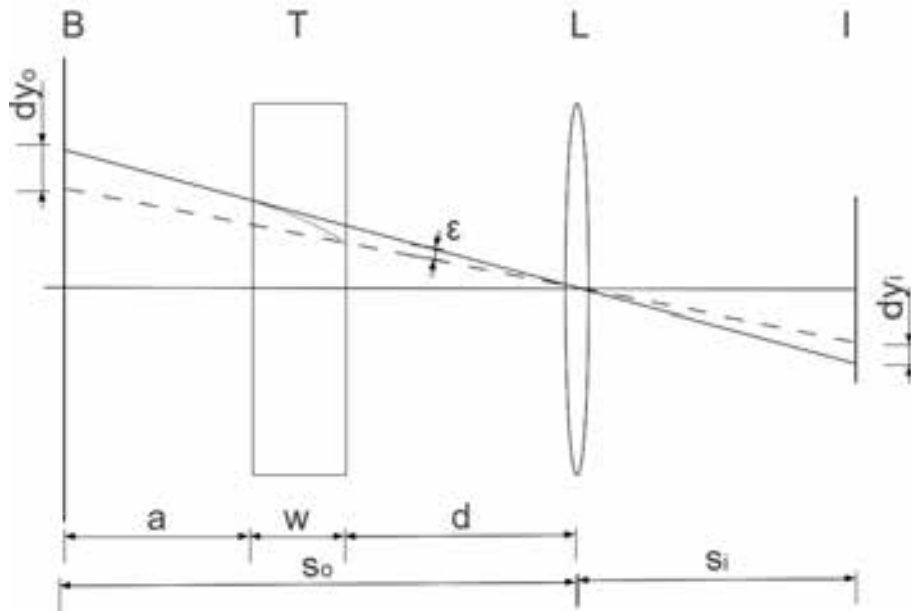


Figure 1. A meridional plane of a BOS setup: B – the background, T – the test section where the fluid flows, L – the imaging lens focused on the background, I – the image plane, coplanar with the recording sensor. The full line indicates the light ray during the imaging of the reference image, while the dashed line illustrates the deflection of the ray in the test section and shows the ray position during the measurement image.

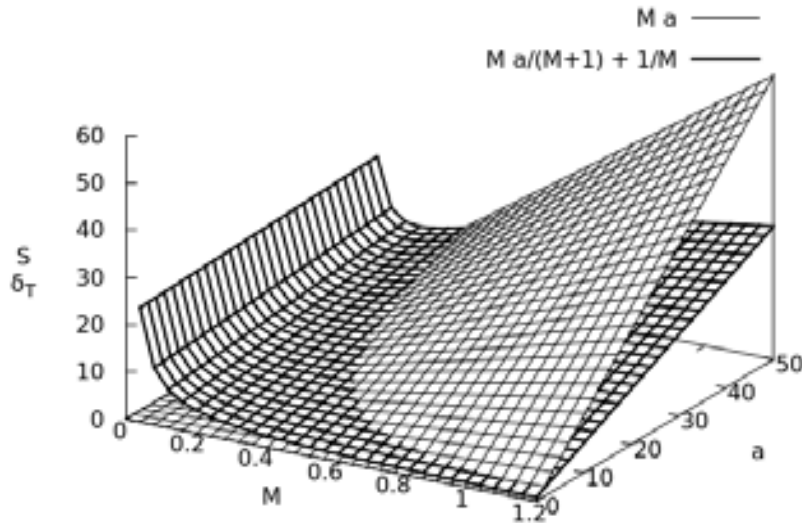


Figure 2. Surface plot of the sensitivity S (thin line, Eq. 6) and uncertainty δt (thick line, Eq. 7) of a BOS system for unit values of $f_{\#}$ (f-number of the lens) and Δpx (linear dimension of the pixel size). For small magnifications, uncertainty plays the determining role in adjusting the system, while for large magnifications, the system can be made quite sensitive. In practice, $f_{\#}$ is 5.6-32, while $\Delta px \approx 10 \mu\text{m}$.

Gaussian interpolation. Interrogation windows usually are smaller than 1/10th of the overall image size and have at least three - four dots.

BOS is a line-of-sight integrating technique that gives the 2D projection of the density field. Its spatial and temporal resolutions depend on the optical setup and instruments used, while its sensitivity and accuracy depend - in addition to the above, - on the density gradients in the flow that is being imaged. Determination of temporal resolution of BOS is pretty easy, because it depends on the camera's exposure times. Spatial resolution, on the other hand, requires more careful analysis. Referring to Fig. 1, the smallest detectable dot shift in the image plane is dy_i , in the best case scenario equal to 0.1 px, which physically can be a fraction of a micrometer. The apparent background dot shift, defining the spatial resolution of the system, is the product of this value to the magnification of the system $M=s_o/s_i$,

$$dy_o = M dy_i = M a \varepsilon \quad (5)$$

The sensitivity S of a BOS setup, defined as the smallest detectable angle of deflection ε , in paraxial approximation with $s_o \gg w$, is expressed as

$$S = M a \quad (6)$$

Thus, the sensitivity increases by having an optical system with large magnification, achieved by using longer focal length lenses on cameras with high pixel count, as well as by setting the test section closer to the lens and the background further from it, i.e adjusting for big numerical value for a and small for d . But, since the lens is focused on the background, distance d between the test section and the lens is limited by the blur. The blur is quantified as the increase of the dot area in the image plane and can be neglected only if the blurred dot size is much smaller than the interrogation window during image evaluation process. Combination of the blur diameter and the interrogation window size defines the measurement uncertainty δ_i . Since the imaging sensor is made of a rectangular grid of pixels, each integrating the light acquired from the incident cone, a point from the background is imaged into an area corresponding to the size of the pixel Δ_{px} . Thus, the image gives a discretized picture of the field of view, a feature that provides the lower limit for the spatial resolution of the BOS system. Numerically, this value is

$$\delta_i = \frac{M}{M+1} \frac{a}{f_{\#}} + \frac{\Delta_{px}}{M} \quad (7)$$

where $f_{\#}$ is the f-number of the lens. Figure 2 shows the plot of the sensitivity S and uncertainty δ_i as functions of magnification M and distance background-flow field a for unit values of $f_{\#}$ and Δ_{px} .

Image quality and instrumentation

Image quality characterizes the output achieved by the image recording system (the combination of the camera and the lightning), compared to an ideal image, usually produced numerically on computer. Determination of image quality is largely a subjective matter, but it can be judged based on several general factors, such as noise, dynamic range, sharpness, and contrast and brightness ranges. BOS images present an easier task for image quality determination, because these images are random dots scattered over the field of view; hence, the structural similarities of the compared images do not play a crucial role for image quality determination. In fact, their role becomes the most important, once the recording system is decided, and are evaluated by cross-correlation.

The speed with which a fluid flows determines the shutter speed (exposure time) that the camera needs to operate with, and this proves to be one of the most demanding factors in choosing an image sensor. Shock waves in a shock tube, for example, can be imaged only with scientific grade high-speed cameras, such as Imacon DSR200 or Shimadzu HPV-1, which are capable of imaging at times shorter than 1 μ s. Slow flows that can reach a pseudosteady state, such as slow cooling by natural convection, can be imaged with standard DSLR cameras. In these later cases, exposure time is not a limiting factor, because it can be large enough to reach an average value of temperature reading smaller than the measurement uncertainty, but still be orders of magnitude smaller than the temperature measurement steps. Thus, one would be free to choose a camera with a high pixel count or a large sensor size, so that the image detail is satisfactory for precise measurements. Images shown in Fig. 3 are from both types of high speed cameras and show a detail of the same background imaged through the test section of a shock tube. If one considers the sensitivity of a BOS setup based on the geometry of the layout and the size of the image sensor, Imacon camera would be preferable to Shimadzu, for two reasons: larger pixel

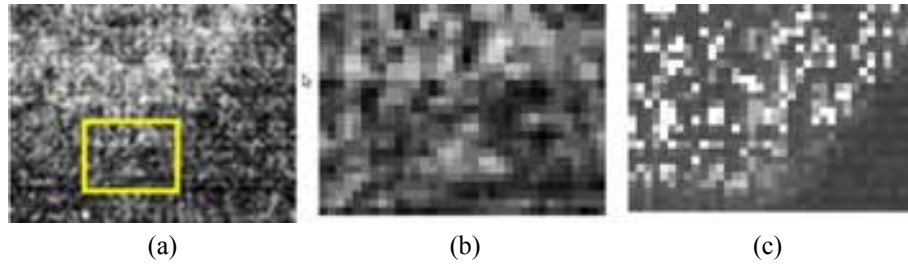


Figure 3. Images (a) and (b) – the latter being the framed part of the former, - are taken with Imacon DSR200 camera, and (c) with Shimadzu HPV-1. Images (a) and (c) show the same field of view, while (b) and (c) have the same pixel count.

count (1200×980 pixels for Imacon vs. 312×260 pixels for Shimadzu), and smaller pixel size ($\approx 10 \mu\text{m}$ vs. $\approx 60\mu\text{m}$). But, despite the facts that the shown field of view is the same and that the images were taken with the same lens as well as under the same illumination, obtained images are quite different, which fundamentally comes about due to the different quantum efficiencies of the respective image sensors. A dramatic outcome of this difference is that the direct (without any processing) evaluation with cross-correlation of images captured by Imacon camera could not give any meaningful results, while images captured by Shimadzu did, as illustrated later. The difference can be explained through different response to luminance of the image sensors and the contrast values of the output file. Both cameras have a sensor with 10 bit dynamic range and give comparable dark images, but the histogram of the measurement images, shows that the Shimadzu camera produces a better contrast.

To quantify the quality of the images obtained by these cameras, we calculated the modified universal image quality index Q' , as proposed by Wang and Bovik [9]. As it is well known, an image is a vector or grayscale values x_i , therefore we can determine image's average $\langle x \rangle$ and standard deviation σ_x . If x is the measurement image (the image for which the quality index is being determined) and y is the ideal reference image (the background produced on computer), then the original definition of universal image quality index Q is given by

$$Q = \frac{\sigma_{xy}}{\sigma_x \sigma_y} \frac{2\bar{x}\bar{y}}{\bar{x}^2 + \bar{y}^2} \frac{2\sigma_x \sigma_y}{\sigma_x^2 + \sigma_y^2}, \quad (8)$$

where

$$\sigma_{xy} = \Sigma \frac{(x_i - \bar{x})(y_i - \bar{y})}{N_{px} - 1}. \quad (9)$$

The universal image quality index Q is made of three terms: the first one corresponds to the correlation between images x and y , the second term gives the response to luminance, and the third term describes the contrast. The closer the image x is to the ideal y , the closer is the value of Q to 1, for each individual term, while complete discrepancy would give $Q=-1$. Since the background image is a high frequency random distribution of dots, the first term for all images is very close to 0, and the image quality index can be modified to take into account only the second and the third terms, namely

$$Q' = Q_L Q_C = \frac{2\bar{x}\bar{y}}{\bar{x}^2 + \bar{y}^2} \frac{2\sigma_x \sigma_y}{\sigma_x^2 + \sigma_y^2}, \quad (10)$$

where Q_L and Q_C are the values for luminance and contrast, respectively. These values for the employed cameras in the experiments described below, are given in Table 1.

Table 1. Luminance and contrast image quality indices for high speed cameras (Imacon, Shimadzu) and standard DSLR cameras (Pentax K-5).

	QL	QC
Imacon DSR200	0.18	0.07
Shimadzu HPV-1	0.62	0.54
Pentax K-5	0.99	0.71

The imaging of high speed flows, such as shock waves, is constrained by the requirement of instrumentation with superior time response, such as high speed cameras. This has the drawback that the quality of the images obtained is not so high. The imaging of natural convection was done with a Pentax K-5 DSRL camera, and, as it is expected, it performs much better, demonstrated by the high values of QL and QC . Therefore, a preliminary investigation of the cameras used for BOS can be done by determining Q' (specifically, QL and QC): a fixed value that would qualify an image as useful or not-useful for image analysis is impossible to be given, but a reasonable judgment can be given based on how close the luminance and contrast terms of Q are to 1, and the main factor effecting low image quality (luminance or contrast) can be diagnosed.

Image evaluation by cross-correlation

In quantitative evaluation of flow visualization, the measurement of several parameters is quite straight forward, e. g. a and d , from Fig. 1. Since the required end result is density field, this can be achieved by determining d_{yi} , which, in turn, is done only through image evaluation. Several techniques for image evaluation exist, but the majority of BOS studies rely on cross-correlation, which consists on defining subsets of the measurement image, representing the interrogation window (IW), and comparing their intensity fields to all equal in size subsets in the reference image. The output of cross-correlation for a prearranged IW is a vector \mathbf{d} , with magnitude and direction corresponding to the shift of the correlation peak. Applying a three point Gaussian peak detection scheme, this vector can be determined with an accuracy of better than 0.1 pixel. The magnitude of \mathbf{d} is the amount of pixel shift of a background pattern due to light deflection, d_{yi} . The number of independent vectors, thus, the evaluated spatial resolution, depends on the size of IW.

There are several sources of uncertainties in flow visualization measurements, which can be divided into two main categories:

1. those due to specifications of instruments, and
2. those that arise from image analysis.

In practice, the dominant type of uncertainties belong to the second type, because the arrangement of the instrumentation in a BOS setup allows for adjustments of sensitivity and spatial resolution to higher levels than those achieved by image analysis.

Displacement vector obtained by image analysis is influenced by IW, background pattern size, spatial frequency of pattern structure, and gradients within IW, which are responsible for error sources such as peak locking, pattern smoothing, etc. The effect of each factor is investigated by applying a step function to a synthetic image, and evaluated with the same procedure as evaluated BOS images. Half of a 128 x 128 pixels synthetically generated reference image of randomly distributed dots is shifted for a number of pixels, giving the simulated measurement image. In other words, the image is sliced in two equal parts, with the right side (pixels in horizontal locations 64 and higher) slid for one or more pixels to the left. Then, the simulated reference and measurement images are cross-correlated by using the PIV plugin for ImageJ [10] and [11]. The effects were observed by the changes on the step function response width (SFRW), as defined in [12].

Image evaluation with different IW shows that the smaller the IW the closer the evaluated jump is to the real step function, as shown in Fig. 4. In this investigation, the simulated images had a dot the size of a pixel, and the image coverage by dots was 50%. The spread and gradual increase of the discontinuity means that there can not be an independent shift vector within the length it takes the evaluated pixel shift value to jump. Therefore, the evaluated spatial resolution for IW=32 is about 36 px, and for IW=8 it is about 10 px. Multipass evaluation with successively smaller IW did not show any improvement in the evaluation of the jump, while it gave erroneous (fluctuating) values for the amount of the pixel shift.

The preparation of the background involves determination of the dot size, frequency (in terms of the number of dots in the field of view), and coverage. While in experiments with natural backgrounds the experimenter has no control over the background features, in experiments under laboratory conditions (e. g. shock tube or wind tunnel experiments), the experimenter can prepare a background that optimizes the measurement based on the camera specifics and the field of view. Figure 5 shows the effect of the dot size in the resolution, where dot sizes δ_d equal to one and four pixels are compared after images are treated by a one pixel step function. The evaluation does not show any large effect on the resolution, but it does give different values for the pixel shift. For the case with $\delta_d = 4$ px, the effective shift of the image corresponds to a quarter of a dot, hence some pixels

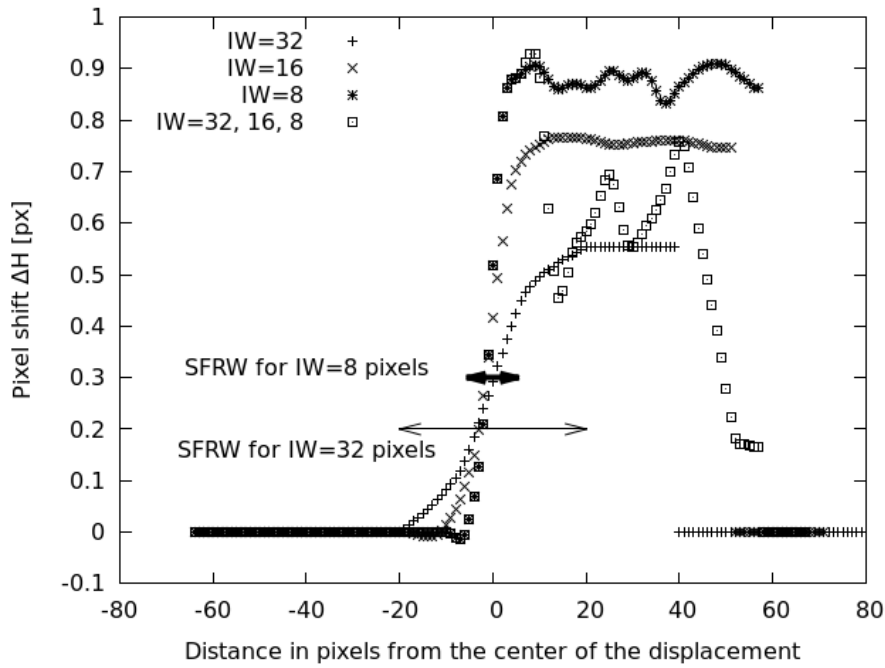


Figure 4. The resolution of the evaluation of a one pixel shift as a function of different sizes of IW. The case for IW = 32, 16, 8 pixels, shows the multipass evaluation. SFRW for extreme cases is also displayed.

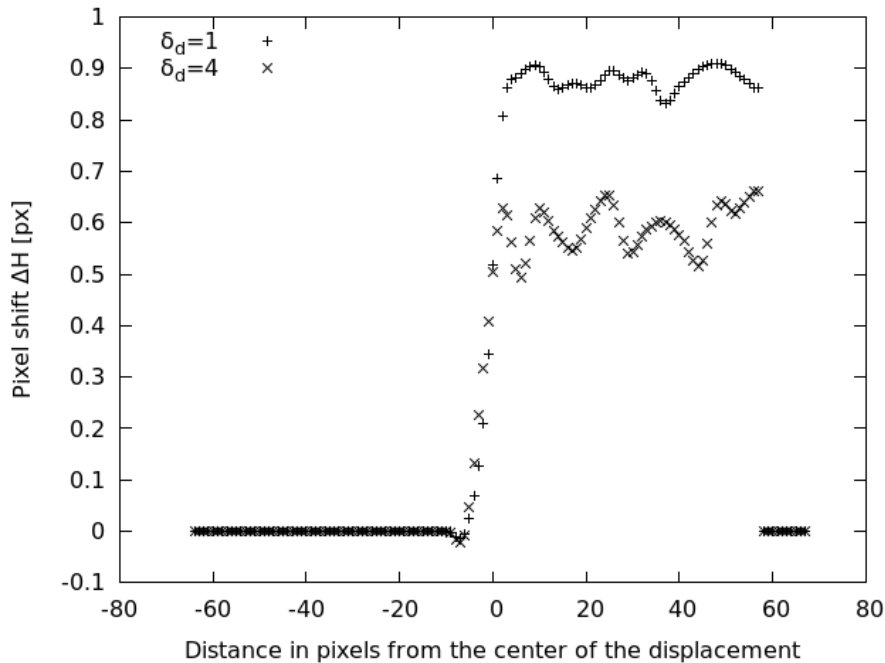


Figure 5. The effect of the dot size on pixel shift. Images with a dot size of one pixel and four pixels are shifted for a pixel and cross-correlated. The SFRW is virtually the same for both cases, but the S/N ratio and the pixel shift is different.

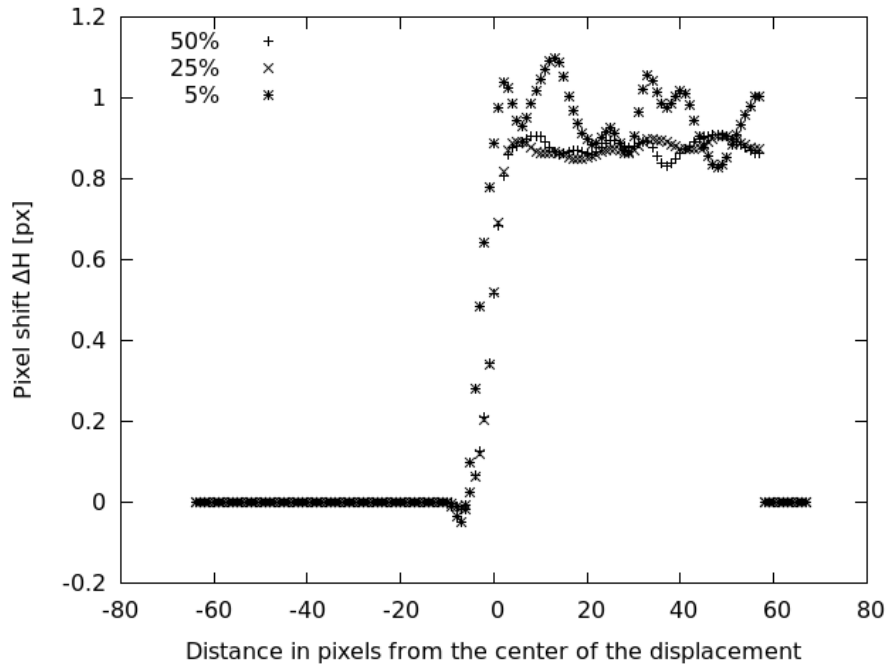


Figure 6. The effect of the coverage of the background by dots. Images covered with black dots of one pixel size are shifted for a pixel and cross-correlated. The SFRW for the images with 25% and 50% coverage are the same, while that for the image with 5% coverage is slightly (but noticeably) larger.

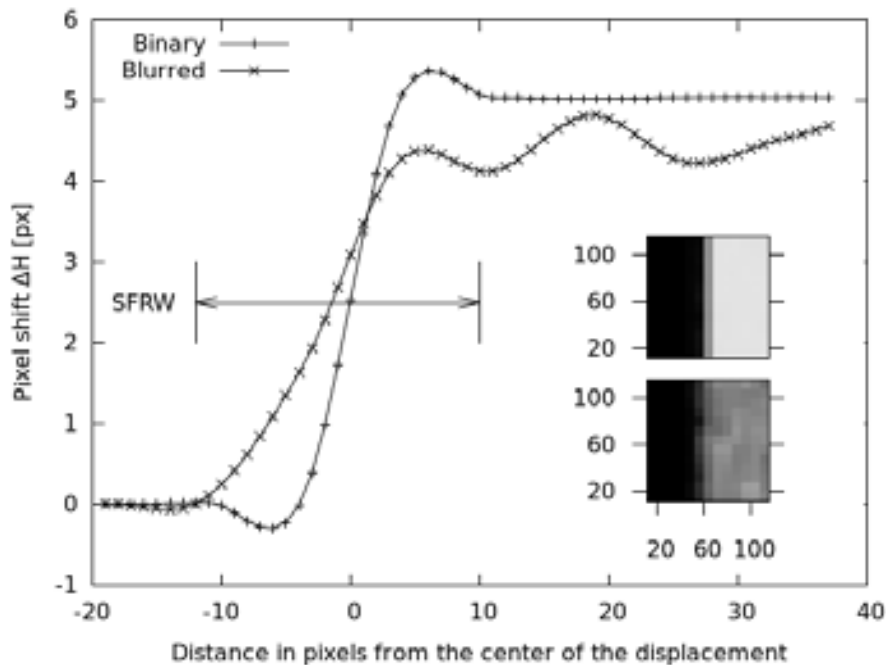


Figure 7. Pixel shift evaluation by cross-correlation ($IW=16$ pixels) of binary (inset, up) and Gaussian blurred (inset, down) synthetic images with dots of one pixel, shifted for 5 pixels. Tics in insets are image pixels. Again, SFRW is virtually the same for both cases, but the S/N changes for the worst in the case of blurred images.

are not recorded as shifted. This situation appears in synthetic image evaluations, because these images have a well defined binary structure. In experiments, an image of a binary background results in a grayscale image with spread histogram peaks around the binary values. This leads to more accurate results during evaluation. Figure 6 shows the effect of dot density, which is defined as the number of dots per unit area of the field of view projected in the total image area. Maximal dot density, 50%, means that half of the image is covered by dots, and the minimal density simulated (5% coverage with dots) is mainly a white featureless background. As previously, the image is treated to a one pixel shift and evaluated with $IW=8$ px. Virtually, there is no difference in evaluating images with dot density of higher than 20-25%, but pixel shift evaluation artifacts start showing for images with lower number of dots. This result is in agreement with the previously published requirement that an IW should have at least four to five dots, each covering 2 pixels [13]. The effect of the blur is investigated by treating the synthetic measurement image with a Gaussian blur of radius of 2 pixels. In this case, the image was shifted for five pixels and the interrogation window was 16 pixels. The effect of the blurring in SFRW is negligible, but this is not so for the determination of the amount of pixel shift. The blurring of the image has the effect of reducing this value for about 10% and introducing fluctuations in its behaviour, thus yielding a lower signal-to-noise (S/N) ratio. This effect comes about because, as compared to the binary image, the blurred image is populated by all possible grayscale values and pattern's spatial frequency is not conserved.

Experimental examples

Two examples of application of BOS to experiments will be given: one for the reflection of a shock wave from an inclined plane (wedge) in a shock tube, and one for the determination of the temperature field during the natural convective cooling.

A BOS experiment for the investigation of shock diffraction and reflection from a wedge (inclined plane) in a shock tube was conducted, with the aim of testing BOS capabilities, because the passage of a planar shock wave is a well studied and documented phenomenon, thus it can serve as a benchmark test. A photo of the experimental setup is shown in Fig. 8. The shock tube was run with air at $p_1 = 0.10$ MPa as the driven gas and nitrogen N_2 at $p_4 = 0.35$ MPa as the driver gas. The model was a stainless steel wedge with the base attached to the top of the shock tube, effectively creating an inclined plane with inclination of 49° . Shock propagation was monitored by three Kistler 603B pressure transducers (only two shown in the figure, the third one being outside of the frame), which also sent the triggering signal for the image recording system. Timing of the experiment was controlled by a combination of an oscilloscope and a pulsed delay generator. Shock Mach number for all experiments was 1.3, and since the effective field of view was 220 mm x 150 mm, a high speed camera was needed for freezing shock's motion. For this reason, two types of cameras were used:

- (i) Shimadzu HPV-1 camera with 312 x 260 pixel count and time resolution of 0.5 μ s, capable of taking 100 images with a maximal frame rate of 1 Mfps. The camera sensor is of the IS-CCD type, with a linear dimension of pixel's light collecting area of about 50 μ m.
- (ii) Imacon DRS 200 camera with 1200 x 980 pixel count and linear dimension of pixel size approximately 6.5 μ m. This camera has 7 channels, each being capable of taking two images with the fastest interframe of 1 μ s, thus resulting in a total of 14 images. Since all 7 channels are independent, their respective interframes can be adjusted freely. The minimal exposure time of the camera is 5 ns, which is faster than the required and used 1 μ s time resolution.

The main differences between these two cameras come from their pixel count, with Imacon having a 10x better characteristic, and the pixel area, with the Shimadzu one having a 10x larger area. The background used in the shock tube experiments was a white sheet with randomly distributed square dots of 1 mm. This background was illuminated by a xenon flashlamp that has pulse duration longer than 1 ms. Although in both experiments the background was a binary image, that is with only white and black areas, the recorded image was an 8 bit grayscale digital file.

The steady temperature field was achieved by a linear tube radiative heater with diameter of 10 mm, length of 150 mm (corresponding to w in Fig. 1), and power of 100 W, placed perpendicularly to the background. Since the field did not change with time, the requirements on the temporal resolution were minimal, so a standard DSLR (Pentax K-5) camera was used. This camera has a sensor of 23.6 mm x 15.8 mm and pixel count of 4928 x 3264 pixels, hence a linear pixel size of ~ 5 μ m. The objective lens had a focal length of 300 mm and experiments were done with aperture of $f/32$. Small apertures were used in order to obtain longer depths of field. Illumination was achieved by back-lighting the printed background with a xenon flashlamp, and the camera exposure times were from 1/180 s. Several types of backgrounds were generated by printing a random dot

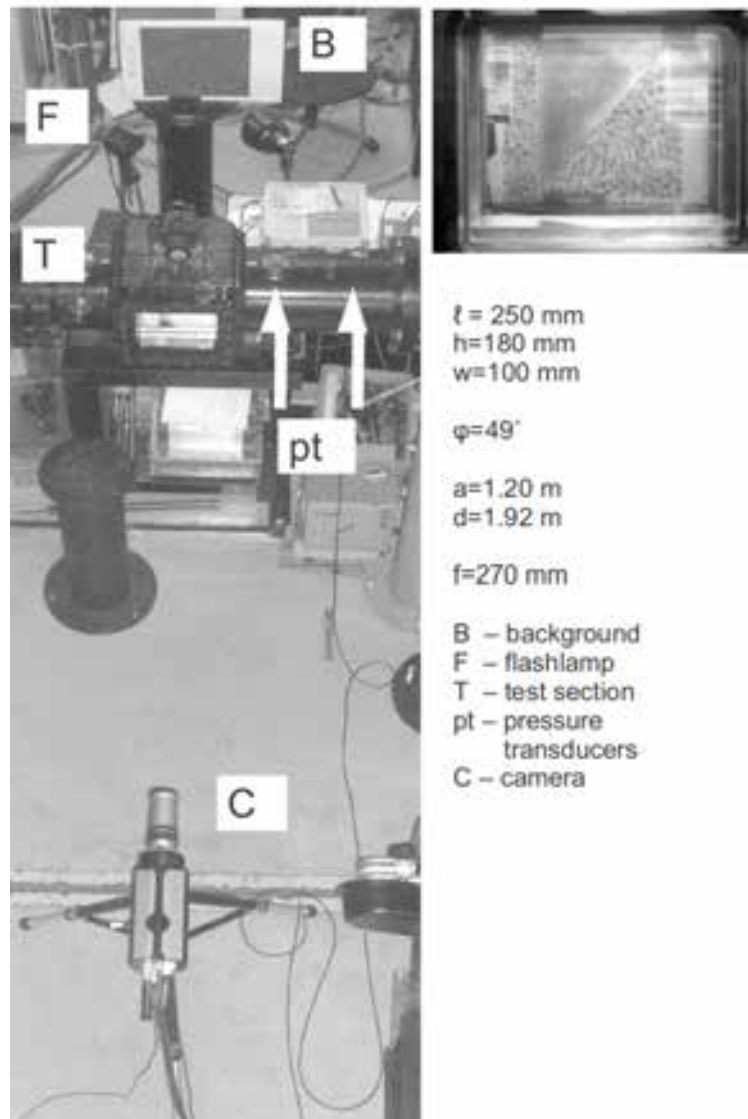


Figure 8. A photo of the experimental setup for the shock reflection experiment, diagnosed by BOS. The inset shows the view of the background from the perspective of the camera C.

pattern in an A4 paper. Setup distances were adjusted to achieve an optical magnification of the system $M=0.1$, with 30 px imaging 1 mm of the field of view. The temperature was simultaneously monitored by 8 thermocouples with temperature resolution of 0.1 K.

The results of these measurements are shown in Figs. 9 and 10. Figure 9 shows the magnitude map of the pixel displacement vector shift. The interrogation window for this evaluation was 8 px, thus giving a resolution of 10 px. Since the optical magnification was 0.1, the measurement uncertainty then is 5 mm. As already stated when the role of the interrogation window was discussed, its large results in the spill of the pixel shifts inside the wedge. Nevertheless, some clear features of the phenomena are observed, such as the shock wave and its reflection, and probably the acoustic region after the reflection.

While these results for density gradient measurement behind a shock wave in a shock tube are very coarse, mainly due to the low pixel count of the high speed camera, the results of BOS applied to natural convection show fine detail, as given in the inset of Fig. 10. Comparison of temperature evolution by BOS, thermocouple

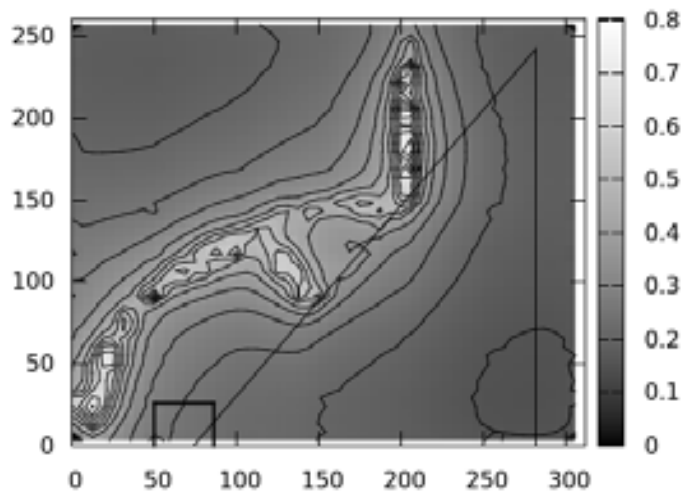


Figure 9. Background oriented schlieren result for the shock reflection from a wedge (black full lines), shown as a magnitude map of vector shift, with pixel locations in coordinates and pixel shift amount in the magnitude bar. The small rectangle starting at pixel (50,0) is the part of the image given in Fig. 3.

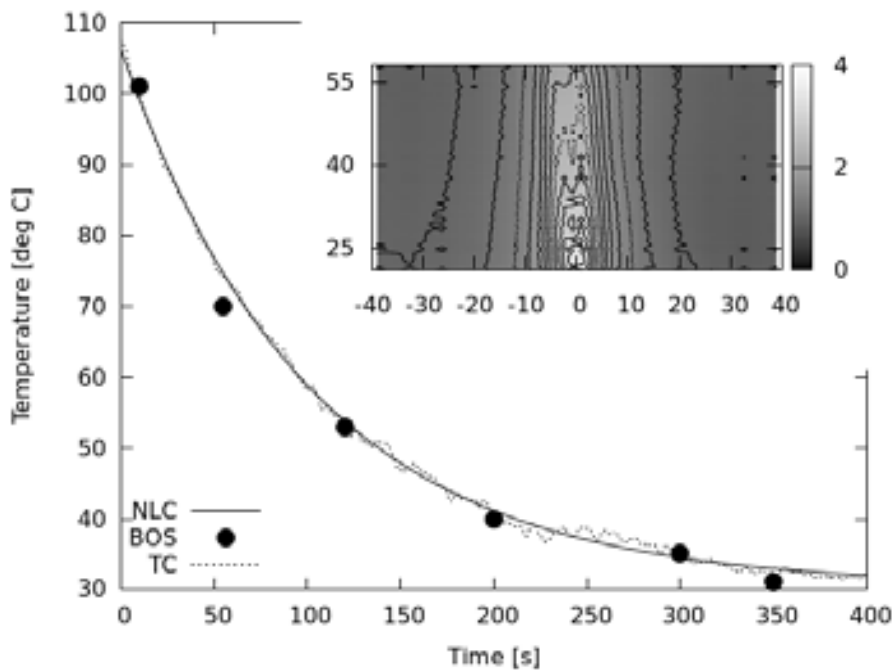


Figure 10. Quantitative BOS result for cooling by natural convection, and the comparison of BOS data to thermocouple (TC) readings and Newton's law of cooling (NLC). Coordinates in the inset give the distance from the center of the heat source, in mm, and the magnitude bar gives the pixel shift.

readings, and according to Newton's law of cooling shows a satisfactory agreement. BOS imaging was done with an extra large pixel count camera (16 megapixels), which had several benefits: a dot covered 8 x 8 px, the dots had five distinct grayscale values, IW was 16 x 16 px. For the sake of computational speed, the image was reduced in size 4 times per direction, giving two pixels per dot. The dot density was 50% and the magnification of the setup was 0.15, with 30 px covering 1 mm of the field of view. Hence, the measurement uncertainty of the BOS technique was estimated to be similar to that of the thermocouples (0.1 K).

Conclusions

The development of background oriented schlieren (BOS) technique is advanced by assessing several factors that influence the extraction of quantitative data, be it in the experimental or image evaluation stage. Introduction of the image quality index is beneficial for simple determination of the instrumentation that would yield desirable and useful images, or for possible diagnostics of the faulty arrangements (illumination or contrast). Investigation of the geometrical arrangement of the instruments used for BOS visualization reveal that arbitrary sensitivity and resolution can be achieved, but, these specifications, though, are later deteriorated by image evaluation. Uncertainties related to the point of measurement are influenced by the interrogation window, defining the spatial resolution of the measurement, while image blurring influences the determination of the pixel shift. BOS technique was applied to two types of flows, with variable success.

Acknowledgment

This work was supported by Global Center of Excellence Program “World Center of Education and Research for Transdisciplinary Flow Dynamics,” Tohoku University, Japan.

References

- [1] G. E. A. Meier: Computerized background-oriented schlieren. *Exp. Fluids*, Vol. 33, pp. 181-187, 2002.
- [2] H. Richard and M. Raffel: Principle and applications of the background oriented schlieren (BOS) method. *Meas. Sci. Technol.*, Vol. 12, pp. 1576-1585, 2001.
- [3] E. Goldhahn and J. Seume: The background oriented schlieren technique: sensitivity, accuracy, resolution and application to a three-dimensional density field. *Exp. Fluids*, Vol. 43, pp. 241-249, 2007.
- [4] S. Tavoularis. *Measurements in Fluid Mechanics*. Cambridge University Press, p. 221, 2005.
- [5] M. J. Hargather and G. S. Settles: Natural-background-oriented schlieren imaging. *Exp. Fluids*, Vol. 48, pp. 59-68, 2010.
- [6] S. B. Dalziel, G. O. Hughes and B. R. Sutherland: Whole-field density measurement by 'synthetic schlieren'. *Exp. Fluids*, Vol. 28, pp. 322-335, 2000.
- [7] O. A. Yevtikhiyeva, N. M. Skorniyakova and A. V. Udalov: An investigation of the error of the background schlieren method. *Measurement Techniques*, Vol. 52, pp. 1300-1305, 2009.
- [8] N. A. Vinnichenko, I. A. Znamenskaya, F. N. Glazyrin and A. V. Udarov: Study of background oriented schlieren method accuracy by means of synthetic images analysis. *Proc. 22nd Inter. Symp. Transport Phenomena*. Delft, The Netherlands, 2011.
- [9] Z. Wang and A. C. Bovik: A universal image quality index. *IEEE Signal Proc. Lett.*, Vol. 9, pp. 81-84, 2002.
- [10] Q. Tseng, E. Duchemin-Pelletier, A. Deshiere, M. Balland, H. Guillou, O. Filhol, and M. Thry: Spatial organization of the extracellular matrix regulates cell-cell junction positioning. *PNAS* Vol. 109, pp. 1506-1511, 2012.
- [11] M. D. Abramoff, P. J. Magalhaes and S. J. Ram: Image Processing with ImageJ. *Biophotonics International* Vol. 11, pp. 36-42, 2004.
- [12] C. J. Kähler, S. Scharnowski, and C. Cierpka: On the resolution limit of digital particle a image velocimetry. *Exp. Fluids* Vol. 52, pp. 1629-1639, 2012.
- [13] M. Raffel, C. E. Willert, and J. Kompenhans: *Particle image velocimetry: a practical guide*. Springer, p. 167, 1998.